Ocean Modelling 39 (2011) 135–145

Contents lists available at ScienceDirect

Ocean Modelling

journal homepage: www.elsevier.com/locate/ocemod

# The effects of the eddy-induced advection coefficient in a coarse-resolution coupled climate model

Riccardo Farneti [a,*], Peter R. Gent [b]

[a] Earth System Physics Section, ICTP, Trieste, Italy
[b] National Center for Atmospheric Research, Boulder, Colorado, United States

ARTICLE INFO

*Article history:*
Available online 2 March 2011

*Keywords:*
Mesoscale eddy parameterisation
Southern Ocean dynamics
Ocean modelling
Climate change

ABSTRACT

The role of the eddy-induced advection coefficient $\kappa$, used in the Gent and McWilliams (1990) parameterisation (GM), is analysed in terms of the response to idealised wind stress perturbation experiments in the GFDL global coupled climate model CM2.1, and compared to solutions with an eddy-permitting version of the same coupled model, CM2.4. The closure implemented in CM2.1 for $\kappa$ is flow-dependent and includes a maximum limit that caps its value. In this paper, we present simulations with a modified version of CM2.1, where the upper limit for $\kappa$ is doubled to 1200 $m^2 s^{-1}$ and the cap to the isopycnal slope $S_{max}$ in GM is also increased to 1/100 from 1/500. These changes allow their product, $\kappa S_{max}$, which is the upper limit to the effect of parameterised eddies, to be an order of magnitude higher than in the original CM2.1 version. Modifications to both GM parameters result in changes in the mean circulation and overall climatology that are non-negligible, which shows that attention has to be paid to the GM implementation during model development. Increasing the value of $\kappa$ does produce a stronger compensation between mean and eddy-induced meridional overturning circulations under stronger wind stress forcing, but the residual circulation response is still stronger than in the eddy-permitting model CM2.4. We show that spatially varying $\kappa$, both in the horizontal and vertical directions, is necessary for a correct simulation of the response to changes in the wind stress. New and improved closures for $\kappa$ are needed, and should be tested in coupled climate models.

© 2011 Elsevier Ltd. All rights reserved.

## 1. Introduction

The Southern Ocean plays a crucial role in setting the global ocean circulation through the large transport of the Antarctic Circumpolar Current (ACC) and its meridional overturning circulation (MOC). The unbounded channel that characterises the Southern Ocean gives rise to climatically important exchanges between ocean basins, formation and ventilation of water masses and air-sea exchanges of heat, freshwater and trace gases such as $CO_2$ (Rintoul et al., 2001; Le Quéré et al., 2007). A dominant influence on oceanic uptake of heat and the global carbon cycle (Mignone et al., 2006) gives the ACC region a central role in the climate system. The Southern Hemisphere (SH) winds that are partly responsible for driving the ACC and MOC have strengthened in the last decades (Gillette and Thompson, 2003). Changes in the Southern Hemisphere are more pronounced than in the Northern Hemisphere because the effect of warming is augmented by the depletion of ozone over Antarctica (Kushner et al., 2001). Because of the important role played by the Southern Ocean in the global climate, it is crucial to accurately simulate its circulation both under present-day conditions and future climate change projections.

Mesoscale ocean eddies make a first order contribution to the dynamical and thermodynamical balance of the Southern Ocean. In this region, the vertical structure is set by eddy dynamics, as eddies transport momentum downward and generate the exponential velocity profile of the ACC system (Ivchenko et al., 2008). Eddy dynamics also sets the strength of the Southern Ocean MOC, as they are known to partially counteract the directly wind-driven Ekman contribution, resulting in a net overturning that is a balance between the two circulations (Marshall and Radko, 2003). The effects of mesoscale eddies are usually parameterised in coarse-resolution ocean climate models with the Gent and McWilliams (1990) formulation (hereafter GM) as an additional eddy advection of tracers. The strengths of isopycnal mixing and eddy-induced advection are set through coefficients which are often set to constants. As the GM coefficient of eddy-induced advection $\kappa$ has a strong influence on the dynamical properties of the Southern Ocean, and hence on its control of the global climate, values are chosen in order to reproduce the best possible present-day climate within each coupled climate model. For modelling future climate change and possible past climates,

* Corresponding author. Tel.: +39 0402240225.
*E-mail address:* rfarneti@ictp.it (R. Farneti).

1463-5003/$ - see front matter © 2011 Elsevier Ltd. All rights reserved.
doi:10.1016/j.ocemod.2011.02.005

however, it would seem necessary to change the coefficient accordingly or, more appropriately, incorporate spatially and time varying coefficients.

Large spatial variations in $\kappa$, in both the horizontal and vertical directions, have already been diagnosed (Karsten and Marshall, 2002) and modelled (Ferreira et al., 2005; Eden, 2006; Eden et al., 2009). The need for a spatially-varying eddy transfer coefficient $\kappa$ was already noted in Gent et al. (1995) and many closures have been proposed since (e.g., Visbeck et al., 1997; Danabasoglu and Marshall, 2007; Eden and Greatbatch, 2008). Table 1 shows the coupled models used in the World Climate Research Program (WCRP) Coupled Model Intercomparison Project 3 (CMIP3) multi-model dataset that use a variable $\kappa$ in their parameterisation of eddy-induced advection. Different closures are used, but what stands out is that, of the 25 coupled models that contributed to the project, only eight have implemented some kind of spatially-varying eddy coefficient. The eight models shown in Table 1 could be further clustered into only four base ocean models. Hence, although theoretical and process studies have shown the importance of spatially-varying closures for $\kappa$, it seems that global coupled modelling is lagging in the implementation of these new closures.

Recently, Farneti et al. (2010) compared results of adding a large perturbation to the zonal wind stress over the Southern Ocean area in two Geophysical Fluid Dynamics Laboratory (GFDL) climate models. The first model used was CM2.1, where eddy effects are parameterised following GM with a closure for $\kappa$ related to properties of the mean flow. The second model, CM2.4, which is a finer-resolution version of CM2.1, is an eddy-permitting model and no parameterisation of mesoscale eddies is implemented. Significant differences were found in both the ACC and MOC of the Southern Ocean when comparing the two GFDL models, with an apparent insensitivity of the circulation to strengthened winds in the fine-resolution coupled model not being reproduced by the coarse-resolution version. Further, Farneti and Delworth (2010) demonstrates that these crucial differences have implications for the evolution of the global ocean circulation. A general conclusion of Farneti et al. (2010) is that, although $\kappa$ is allowed to vary as described in Section 2, the implementation of the GM scheme in GFDL models seems to fall short in reproducing the response of eddy fluxes under changing surface forcings. Although variable, the coefficient $\kappa$ in the CM2.1 GM implementation is capped at the value of 600 $m^2/s$. This is also the value of $\kappa$ used in the ocean component of version 3 of the Community Climate System Model (CCSM3). Therefore, this value of $\kappa$ is appropriate to obtain a realistic simulation of the present day ACC and overall Southern Ocean dynamics in a coarse-resolution model; indeed CM2.1 and CCSM3 rank amongst the best coupled models in terms of reproducing the SH westerly winds and ocean circulation (Russell et al., 2006; Sloyan and Kamenkovich, 2007). We also note from Table 1 that the GFDL models are at the bottom end of the table in terms of values of $\kappa$.

**Table 1**
List of CMIP3 coupled models that use a spatially varying coefficient $\kappa$ (in $m^2\,s^{-1}$) for the parameterization of eddy-induced transports. Given, if found in the literature, are the minimum and maximum values allowed within each model and the type of closure the model refers to (∗ = value not publicly available).

| AOGCM | Ocean model | Formulation of GM | $\kappa$ ($m^2/s$) |
|---|---|---|---|
| 1. UKMO-HadCM3 | HadOM3 | Visbeck et al. (1997) | 300–2000 |
| 2. UKMO-HadGEM1 | HadGOM1 | Visbeck et al. (1997) | 150–2000 |
| 3. INGV-SXG | OPA8.2 | Treguier et al. (1997) | 15–2000 |
| 4. IPSL-CM4 | OPA8.1 | Treguier et al. (1997) | 15–2000 |
| 5. GFDL-CM2.0 | MOM3 | Griffies et al. (2005) | 100–600 |
| 6. GFDL-CM2.1 | MOM4 | Griffies et al. (2005) | 100–600 |
| 7. CSIRO-MK3.5 | MOM2.2 | Visbeck et al. (1997) | ∗ |
| 8. GISS-ER | Russell | Visbeck et al. (1997) | ∗ |

Implicit in the comparison between the two GFDL models is the fact that CM2.4 is assumed to give the correct response to the large wind perturbation, even though its resolution 'permits' eddies rather than resolving them. Very recently, Viebahn and Eden (2010) have addressed the impact of eddies on the response of the Southern Ocean circulation to climate change using a very idealised ocean model. The Eden and Greatbatch (2008) method is used for their implementation of the GM parameterisation; a method that has been compared to other implementations, including constant $\kappa$, in a low resolution global ocean model in Eden et al. (2009). The regional model in Viebahn and Eden (2010) is 1 km deep with a flat bottom and idealised land masses, but it does use 5 km resolution, which is considered to resolve the eddies at those latitudes. One of their results, shown in their Fig. 5, is that the maximum of the residual MOC does increase with increasing resolution, but this increase becomes small at large zonal wind stresses.

We test here the effects of increasing the range of values under which GM can operate in CM2.1 by increasing the maximum value in the closure for $\kappa$. We look at the consequences for the climatology in the control run and repeat the SH wind perturbation experiment described in Farneti et al. (2010). In the latter experiment, more energy input to the flow generates enhanced mesoscale eddy fluxes, which should be better reproduced with a larger $\kappa$. Hence, we test the hypothesis that the response of CM2.1 to a large zonal wind stress perturbation could now be closer to the solution of the eddy-permitting CM2.4. This paper documents results obtained when the cap of 600 $m^2/s$ for $\kappa$ is doubled to 1200 $m^2/s$ in a new integration of the CM2.1 model. The doubling of $\kappa$ is appropriate in light of the large change to the zonal wind stress applied in the perturbation experiment that roughly doubles the maximum value of the zonally-integrated zonal wind stress. We briefly describe the model, experimental design and changes to the implementation of the mesoscale eddy parameterisation in Section 2 and compare results with previous runs of CM2.1 and CM2.4 in Section 3. We discuss our findings in light of the previous modelling efforts, state some possible lines of progress and conclude in Section 4.

## 2. The GFDL CM2.1 and CM2.4 models and experimental design

The ocean component used in CM2.1 has a coarse resolution of 1°, with a progressively finer meridional resolution equatorward of 30° reaching 1/3° at the equator, so that the Gent and McWilliams (1990) parameterisation is used for eddy fluxes. Extensive documentation on the formulation and numerical implementation of GM in the GFDL CM2.1 model can be found elsewhere (Griffies et al., 2005, for example).

In CM2.1, mixing associated with the mesoscale eddy field includes eddy-induced diffusive and advective processes acting on locally referenced isopycnal surfaces (or neutral surfaces). The tracer flux arising from neutral physics is given by $\mathbf{F} = -\mathbf{J}\cdot\nabla C$, where the mixing tensor acting on the gradient of the tracer concentration is given by Griffies (1998)

$$\mathbf{J} = \begin{pmatrix} A_I & 0 & (A_I-\kappa)S_x \\ 0 & A_I & (A_I-\kappa)S_y \\ (A_I+\kappa)S_x & (A_I+\kappa)S_y & S^2A_I \end{pmatrix}. \quad (1)$$

Here, $A_I$ is the along isopycnal diffusion coefficient (set to a constant value of 600 $m^2\,s^{-1}$), $\kappa$ is the eddy transfer coefficient and $\mathbf{S} = -\nabla_z\rho/\partial_z\rho$, is the magnitude of the neutral mean isopycnal slope. We can then express the circulation in terms of a residual-mean streamfunction

$$\Psi_{\text{res}} = \overline{\Psi} + \Psi^*, \tag{2}$$

where the mean flow is driven by Ekman currents and the eddy streamfunction is defined by $\Psi^* = \kappa S$.

Near the surface boundary layer, the neutral slope $S$ can become very large. To avoid unphysical values in the velocity field, the streamfunction is often tapered to the surface following different schemes. In CM2.1, when the neutral slope reaches a critical value set by a maximum slope $S_{max}$, GM skew fluxes are linearly tapered towards the surface within regions of steep neutral slopes. The formulation used for the tapering is

$$\Psi^*(z) = \Psi^*(z = -h)\frac{\eta - z}{\eta + h}, \tag{3}$$

where $\eta$ is the free surface height and $h$ is the depth at which the slope becomes greater than $S_{max}$. This approach ensures an upper limit, $\kappa\ S_{max}$, to the maximum volume flux associated with GM. The choice of $S_{max}$ is dictated by numerical necessities, and is set to 1/500 in the standard CM2.1 configuration. Farneti et al. (2010) found that this value strongly narrows the range of slopes under which GM can freely operate under changing surface forcings, and thus performed a sensitivity study on the $S_{max}$ parameter to better understand the limitations of the GM numerical implementation in CM2.1. The value of possible slopes was raised from 1/500 to 1/100, thereby allowing for bigger eddy-induced fluxes. However, setting the maximum slope $S_{max}$ to the five times larger value produced parameterised eddy fluxes that were still much weaker than in the eddy-permitting CM2.4 simulation.

In this paper, we focus on the role of an equally important parameter, the eddy-induced advection coefficient, given by

$$\kappa = \alpha\overline{|\nabla_z \rho|}^z \left(\frac{L^2 g}{\rho_o N_o}\right). \tag{4}$$

Here, $\alpha$ is a dimensionless tuning constant set to 0.07, $L$ is a constant length scale set to 50 km, $N_o$ is a constant buoyancy frequency set to $0.004\ \text{s}^{-1}$, $g = 9.8\ \text{m s}^{-1}$ is the acceleration of gravity and $\rho_o = 1035\ \text{kg m}^{-3}$ is the reference density for the Boussinesq approximation. In CM2.1, $\kappa$ is set to be proportional to $\overline{|\nabla_z \rho|}^z$, which is the average of the horizontal gradient of locally referenced potential density taken over the depth range 100 m to 2000 m, and it equals the neutral slope times $N^2$. Thus, as originally suggested by Visbeck et al. (1997), $\kappa$ is itself proportional to the neutral slope, so that the resulting eddy-induced transport is proportional to the square of the slope, and thus presumably more sensitive to changes in surface forcing than with a simplest approach of constant eddy transfer diffusivity. In CM2.1 the GM eddy transfer coefficient $\kappa$ is bounded by a minimum value of $100\ \text{m}^2\ \text{s}^{-1}$ and a maximum value that is set to $600\ \text{m}^2\ \text{s}^{-1}$ in the control run used in Farneti et al. (2010).

We present two new simulations in this paper. First, a new control integration (CTLb), which differs from the CM2.1 control integration used in Farneti et al. (2010) (here referred to as CTLa) only by the maximum value set for the two parameters $\kappa$ and $S$. In CTLb $\kappa$ is capped at $1200\ \text{m}^2\ \text{s}^{-1}$ and $S_{max}$ is set at 1/100. The previous run of CTLa used $600\ \text{m}^2\ \text{s}^{-1}$ and 1/500 respectively (see Table 2). CTLb is 100 years long starting from year 101 of CTLa. Although the global ocean circulation will adjust on centennial time scales to the change in activity of parameterized eddies, a control length of 100 years is sufficient to show a significant sensitivity to the GM parameters. Then, we repeat for CTLb the SH momentum flux perturbation experiment performed on CTLa. In this case, an anomalous wind stress pattern is added to the wind stress felt by the ocean between latitudes 20° S and 75° S. The wind stress anomaly is derived as the difference in the late 21st century between a CM2.1 simulation with A1B radiative forcing and the control simulation. The anomaly is constant in time and multiplied by a factor of 3 (Farneti et al., 2010). The perturbation experiment SHW3Xb is 100 years long starting from year 101 of CTLa, just like the CTLb run.

**Table 2**
Main parameters in the numerical implementation of GM in the GFDL CM2.1 model. $A_l$ is the along isopycnal diffusion coefficient, $\kappa$ is the eddy transfer coefficient and $S_{max}$ is the maximum isopycnal slope. Values shown are for the two control runs, CTLa and CTLb, and their respective perturbation experiments.

| Parameter | CTLa | CTLb |
|---|---|---|
| $A_l$ ($\text{m}^2\ \text{s}^{-1}$) | 600 | 600 |
| $\kappa$ ($\text{m}^2\ \text{s}^{-1}$) | 100–600 | 100–1200 |
| $S_{max}$ | 0.002 | 0.01 |

The oceanic resolution of CM2.4 is 1/4° (~27 km) at the equator and progressively increases towards the poles reaching 9 km at 70°. In contrast to CM2.1, no closure for the eddy fluxes is used in this eddy-permitting model. In this case, we obtain the eddy-contribution to the streamfunction $\Psi^*$ by first binning the time-mean Eulerian transport into the time-mean potential density field, then the eddy-driven circulation is obtained by subtracting the mean component from the residual ($\Psi^* = \Psi_{\text{res}} - \overline{\Psi}$). The CM2.4 SH momentum flux perturbation experiment is 40 years long and, like the CM2.1 simulations, starts from year 101 of its control run. All CM2.1 experiments are analysed and interpreted under the hypothesis that fine-resolution CM2.4 results show a realistic sensitivity of eddy fluxes to surface forcings. Certainly the eddy-permitting resolution of CM2.4 is not adequate to resolve all eddy baroclinic modes, and refining the horizontal resolution could modify the modelled eddy compensation to Ekman transport changes. Therefore, it is imperative to make progress in the closure for mesoscale eddy activity.

## 3. Results

We begin by comparing the spatial distribution of $\kappa$ in the Southern Ocean area for the two control runs of CM2.1: CTLa and CTLb. From Fig. 1 we can clearly infer a strengthened eddy-induced advection in CTLb due to the larger values of $\kappa$, which is now capped at $1200\ \text{m}^2\ \text{s}^{-1}$. We note that the closure for $\kappa$ in CM2.1 is independent of depth, i.e. $\kappa(x,y,t)$, and the same values are used throughout the water column. Doubling the cap for $\kappa$ has produced stronger maxima in the Southern Ocean, where regions of strong eddy activity like the Pacific sector, Drake Passage and Agulhas region are now saturated at $1200\ \text{m}^2\ \text{s}^{-1}$. It is possible that these maxima could further intensify with a larger cap on $\kappa$ under the same forcings. Similar behaviour is found in other regions of large eddy transport like boundary currents.

### 3.1. Changes in the control run climatologies

The value of $S_{max} = 1/500$ was originally chosen in order to better reproduce the Southern Ocean convection and ventilation of climatically important tracers (Gnanadesikan et al., 2006). The sensitivity of the coupled model to the maximum slope is further documented in Gnanadesikan et al. (2007a), showing indeed a significant shallowing of mixed layer depth, reduction of ventilation and heat uptake as well as changes in surface temperature with $S_{max} = 1/100$ as in this study. Then, the CM2.1 value of $600\ \text{m}^2\ \text{s}^{-1}$ for $\kappa$ ensured the desired strength of eddy-induced volume and heat transport as $\kappa S_{max}$ represents the upper limit for the volume flux associated with GM in the model, which in this case equals to $1.2\ \text{m}^2\ \text{s}^{-1}$ (Griffies et al., 2005).

CTLa and CTLb differ in both the upper limit on $\kappa$ and the value of $S_{max}$ and the two changes are expected to produce

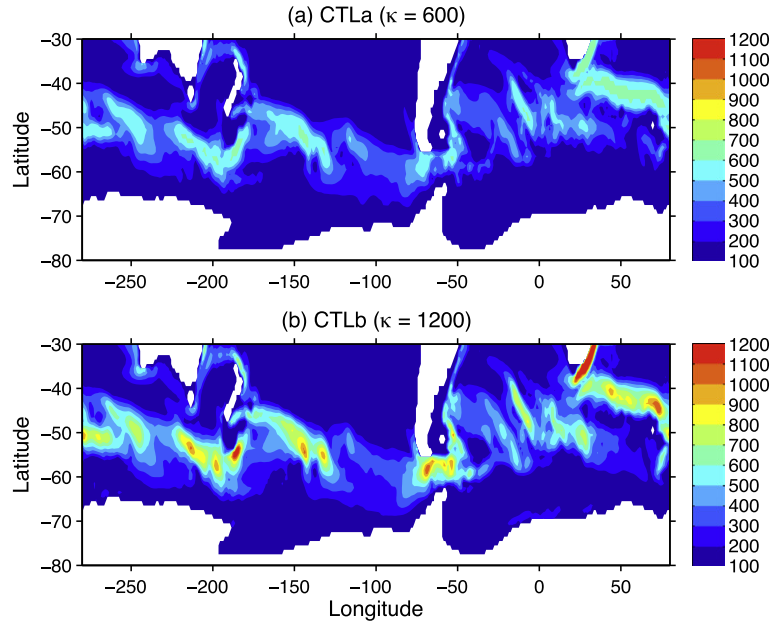


**Fig. 1.** GM eddy-induced advection coefficient $\kappa$ ($m^2\,s^{-1}$) for the two CM2.1 control experiments. (a) CTLa with an upper limit of $\kappa = 600\ m^2\,s^{-1}$ and (b) CTLb with a doubled upper limit of $1200\ m^2\,s^{-1}$. Values plotted are time-means for years 181 to 200.

non-negligible effects on the ocean structure and its dynamics. Fig. 2 shows the time-mean zonally averaged potential density referenced to the surface ($\sigma_0 = \rho$ [kg m$^{-3}$] – 1000) in the upper Southern Ocean for the two controls. Increasing $\kappa$ for the eddy-induced transport velocity has the effect of flattening the isopycnals, releasing the potential energy stored in the initial tracer front. Indeed, CTLb shows a reduced tilt in isopycnals compared to CTLa (Fig. 2). This state is responsible for a weaker interaction between the upper and deep ocean, and can thus be linked to a weaker ventilation ('older' waters in the model; see also later in the text) and shallower mixed layer depths (not shown). Also, a reduction in the ACC horizontal transport can be inferred through geostrophy (see also Fig. 9). As expected, consequences of varying the GM coefficients are not restricted to the Southern Ocean. The time-mean global MOC is shown in Fig. 3 for both the residual (Eulerian mean plus eddy-induced component) as well as the GM contribution

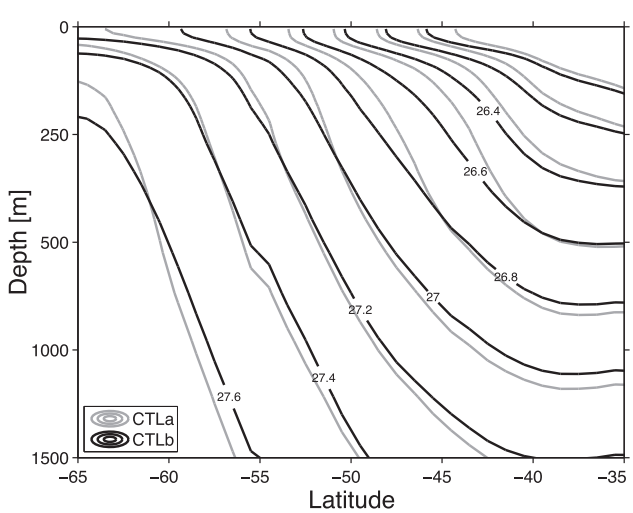


**Fig. 2.** Zonally averaged potential density surfaces referenced to the surface ($\sigma_0 = \rho$ [kg m$^{-3}$] – 1000) in the Southern Ocean region for the two CM2.1 controls, CTLa (grey contours) and CTLb (black contours).

alone in the two controls. While the wind-driven cells remain very similar in both magnitude and structure, we note a reduction in the maximum strength of the North Atlantic MOC (of ~3 Sv; 1 Sv ≡ $10^6\ m^3\,s^{-1}$) and of the SH sub-polar cell which is partially cancelled by the much stronger eddy-induced circulation (Fig. 3d). This is consistent with the Gnanadesikan (1999) model for the large-scale oceanic circulation. Assuming a constant diffusive upwelling of waters through the main subtropical thermocline, then, at steady state, changes to the residual between wind-driven flow and the eddy-induced circulation in the SH will have to balance changes in the Northern Hemisphere sinking flux. As the wind stress across the ACC remains largely unchanged between CTLa and CTLb (not shown), the Ekman northward flux component is also unchanged. Hence, the enhanced opposing eddy-induced transport (allowed by larger $\kappa$ and $S_{max}$) is responsible for a weaker residual circulation in the Southern Ocean, which is matched by a reduced transport in the North Atlantic and subsequent weaker upwelling of waters within the Southern Ocean. The SH deep cell of the overturning circulation is also affected by changes to the GM formulation, and it strengthens with a bigger $\kappa$ in CTLb (Fig. 3b).

Modifications to the parameterised eddy fluxes are also reflected in changes to the meridional heat flux in the ocean. The global and Atlantic heat transports are shown in Fig. 4 for CTLa and CTLb together with two reanalysis products used by Trenberth and Caron (2001) and *in situ* measurements analysed by Ganachaud and Wunsch (2003). More than for previous analyses, it is clear from this metric how difficult it is to find a compromise in the simulated climate when choosing parameter values. The strengthened poleward eddy fluxes are responsible for a heat flux that is now negative at all latitudes in the Southern Ocean for CTLb, and thus more in line with observational estimates. However, the meridional heat transport in the North Atlantic is further reduced from CTLa, and the bias from observations is enhanced there. Hence, changes to the upper limit on $\kappa$ and the value of $S_{max}$ both contribute to non-trivial modifications to the modelled climatology. Our efforts to make GM more responsive to large changes in surface forcings might have actually improved some aspects of the climatological conditions in the coupled model. However, we

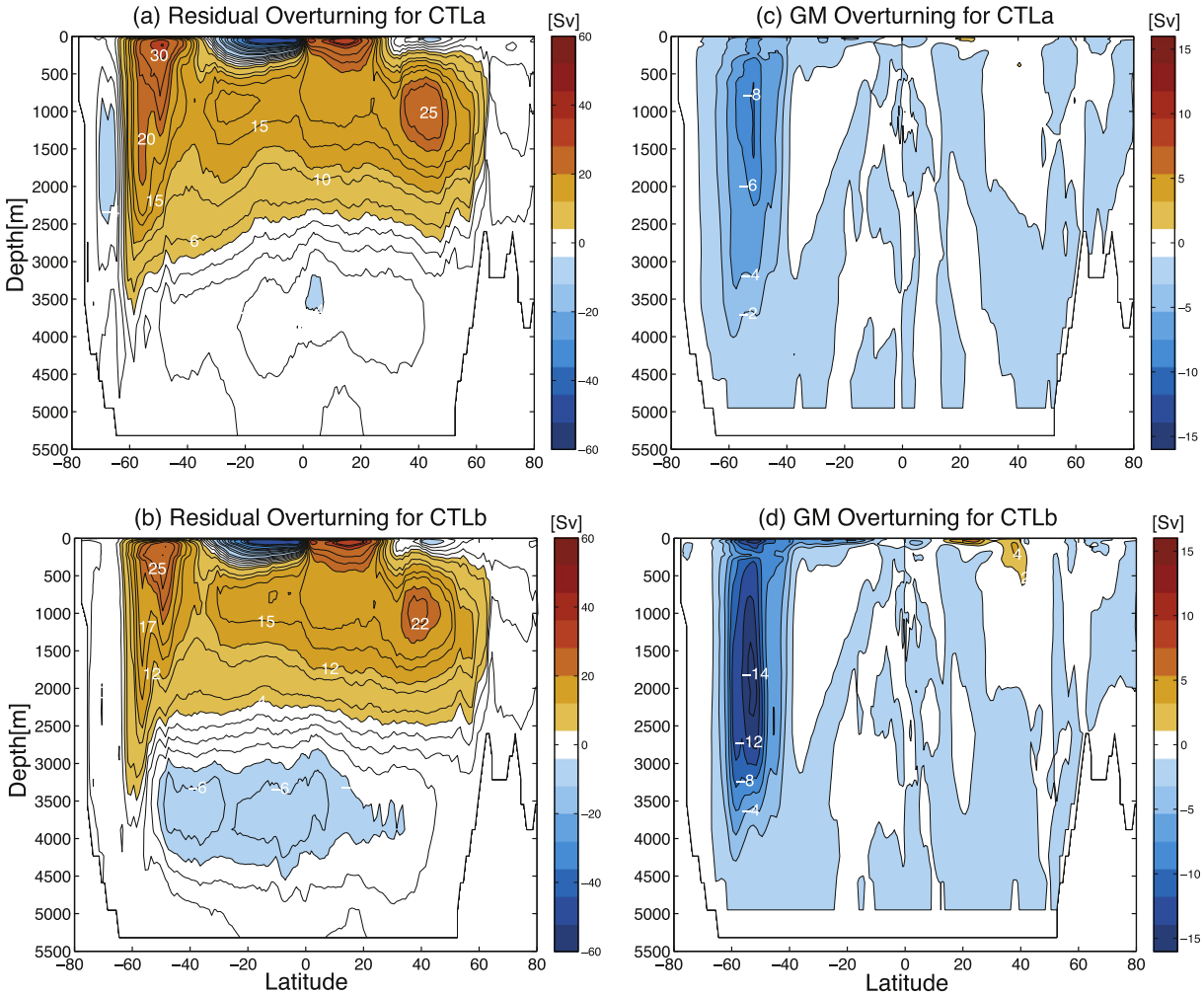


**Fig. 3.** Time-mean residual global MOC in (a) CTLa and (b) CTLb. Both the resolved Eulerian velocity field as well as the eddy driven transport parameterised according to Gent and McWilliams (1990) are included. Relative to the GM parameterisation, $\kappa$ is capped at 600 $m^2 s^{-1}$ and $S_{max}$ is set at 1/500 for CTLa while CTLb has $\kappa = 1200$ $m^2 s^{-1}$ and $S_{max} = 1/100$. Also, the time-mean eddy-driven contribution alone to the global MOC is shown in (c) CTLa and (d) CTLb.

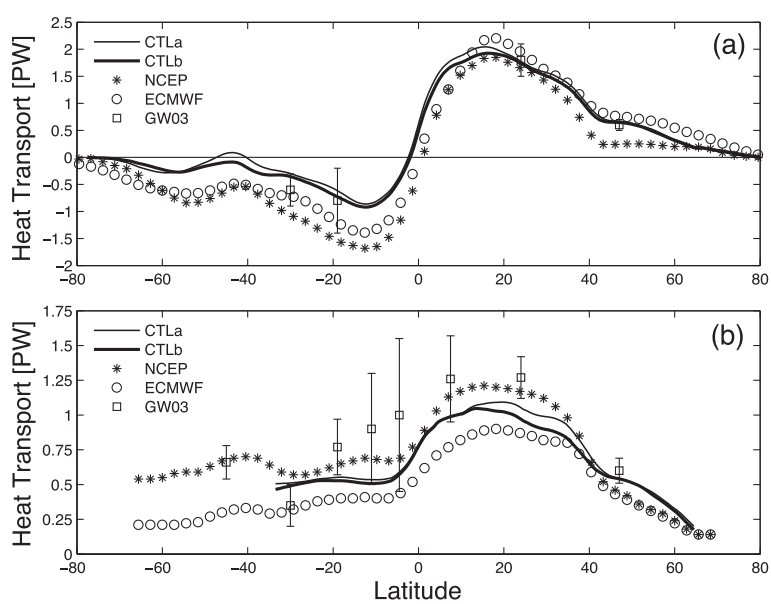


**Fig. 4.** Time-mean ocean heat transport (OHT). Shown are (a) Global and (b) Atlantic basin estimates from the two CM2.1 controls (CTLa and CTLb). Observational estimates are also shown from *in situ* measurements (GW03; Ganachaud and Wunsch, 2003), and the reanalysis estimates from Trenberth and Caron (2001) using both NCEP and ECMWF reanalysis products.

acknowledge that by setting the upper limit of parameterised eddies to be an order of magnitude higher than in the original control we have degraded some important features of the CM2.1 simulation of present-day climate. This is summarized in Table 3, where the root-mean-square (rms) sea surface temperature (SST) and sea surface salinity (SSS) errors are shown for both CM2.1 controls and CM2.4. It is clear from global and regional averages that the proposed changes in GM have worsened the rms errors in CM2.1. The better climatology in CTLa is the reason why the limits on $S_{max}$ and $\kappa$ were chosen in the original setting, and are believed to be the best possible compromise values for the simulation of present-day climate with CM2.1. Note that CM2.4 is also worse in terms of hydrographic errors compared to CM2.1 CTLa, and thus it should not be taken as a better model in every aspect.

**Table 3**
Global and regional root-mean-square (rms) errors for the GFDL coupled models CM2.1 (CTLa and CTLb) and CM2.4 when compared to the observational analysis of Reynolds et al. (2002) and Steele et al. (2001), for SST (in °C) and SSS (in psu) respectively. Large scale pattern features of both SST and SSS biases are persistent across models.

| **SST** | CTLa | CTLb | CM2.4 |
|---|---|---|---|
| Global | 1.17 | 1.29 | 1.29 |
| 90S-30S | 1.27 | 1.41 | 1.38 |
| 30S-30N | 0.97 | 0.94 | 0.99 |
| 30N-90N | 1.49 | 1.7 | 1.8 |
| **SSS** | CTLa | CTLb | CM2.4 |
| Global | 0.87 | 0.98 | 1.01 |
| 90S-30S | 0.39 | 0.52 | 0.54 |
| 30S-30N | 0.74 | 0.75 | 0.92 |
| 30N-90N | 1.57 | 1.57 | 1.66 |

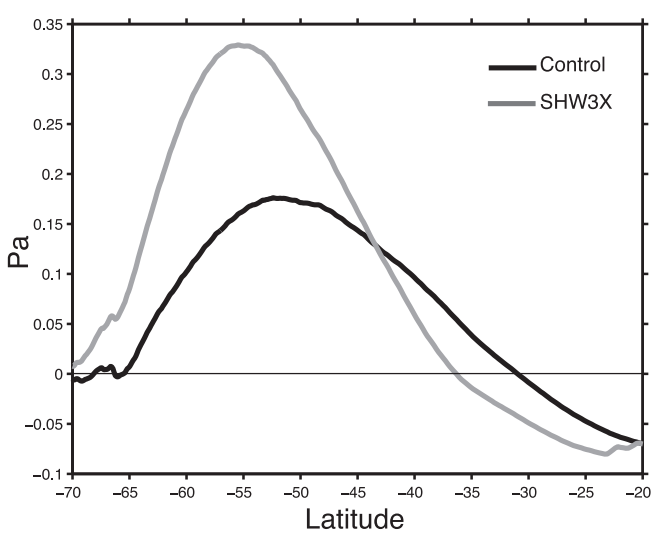


**Fig. 5.** Zonally-averaged wind stress (in Pa) over the ocean. Values are plotted for the control (black) and wind perturbation experiment SHW3X (grey). The SHW3X integration, which is constructed from anomalies obtained by a climate change scenario with the same model, roughly doubles the peak wind stress of the control run.

### 3.2. Wind stress perturbation runs

In this section, we present results from the wind perturbation experiment SHW3Xb and compare with solutions based on CM2.1 CTLa (SHW3Xa) and CM2.4 that are extensively discussed in Farneti et al. (2010). The zonally-averaged wind stress for the control and perturbation integration is shown in Fig. 5, where the large anomaly applied to the ocean model represents roughly a doubling of the peak wind stress in the SH (this is true for both controls and their perturbation runs). Fig. 6 shows the sensitivity of $\kappa$ to the enhanced momentum flux in SHW3Xb. Doubling the surface wind forcing enhances regions already characterised by high levels of eddy activity in the core of the ACC. We note that $\kappa$ is saturated at its maximum level of 1200 $m^2\,s^{-1}$ in many locations throughout the ACC belt, suggesting that the wind forcing applied should be related to stronger eddy fluxes there. The regions of saturated $\kappa$ are also found in SHW3Xa, but in this case at 600 $m^2\,s^{-1}$. That is, the response of CM2.1CTLa to SHW3X forcing is strongly hampered not only by the cap on the isopycnal slope $S_{max}$, as discussed in Farneti et al. (2010), but also by the upper limit on $\kappa$. The two effects give rise to a transport $\Psi^* = \kappa\, S_{max}$ not adequate to reproduce the effective eddy-induced fluxes found in the eddy-permitting CM2.4 simulation under the same forcing.

The effects of an intensification of the wind stress over the SH for the Southern Ocean and global meridional overturning is considered next. Fig. 3 has demonstrated the stronger GM contribution to the overturning when the upper limits for both $\kappa$ and $S_{max}$ are raised. We test whether the eddy-induced MOC ($\Psi^*$) can now change significantly to compensate for the increase in the Eulerian-mean MOC ($\overline{\Psi}$) due to the enhanced northward Ekman flow under SHW3X forcing. We plot the results for CTLb and SHW3Xb in Fig. 7, where the MOC is computed in potential density space for the Southern Ocean latitudes. $\overline{\Psi}$ (middle panels of Fig. 7) increases by 15 Sv, consistent with previous results with CTLa (Farneti et al., 2010). This is the directly wind-driven component, and will thus change proportionally to the wind stress, irrespective of the model formulation. $\Psi^*$, in contrast to SHW3Xa, shows a substantial increase in SHW3Xb of about 8 Sv (bottom panels of Fig. 7). The strengthening of the GM overturning leads to a total change of 7 Sv in the core of the residual circulation $\Psi_{res}$. Thus, the values of the GM parameters chosen for CTLb represent a substantial improvement with respect to the standard CM2.1 setting. In the latter case, $\Psi^*$ showed virtually no sensitivity to the winds,

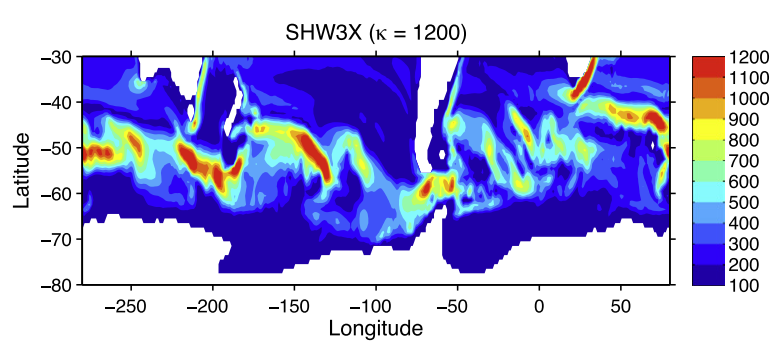


**Fig. 6.** As in Fig. 1 but for the perturbation experiment SHW3X based on CTLb. Note the large areas of saturated $\kappa$.

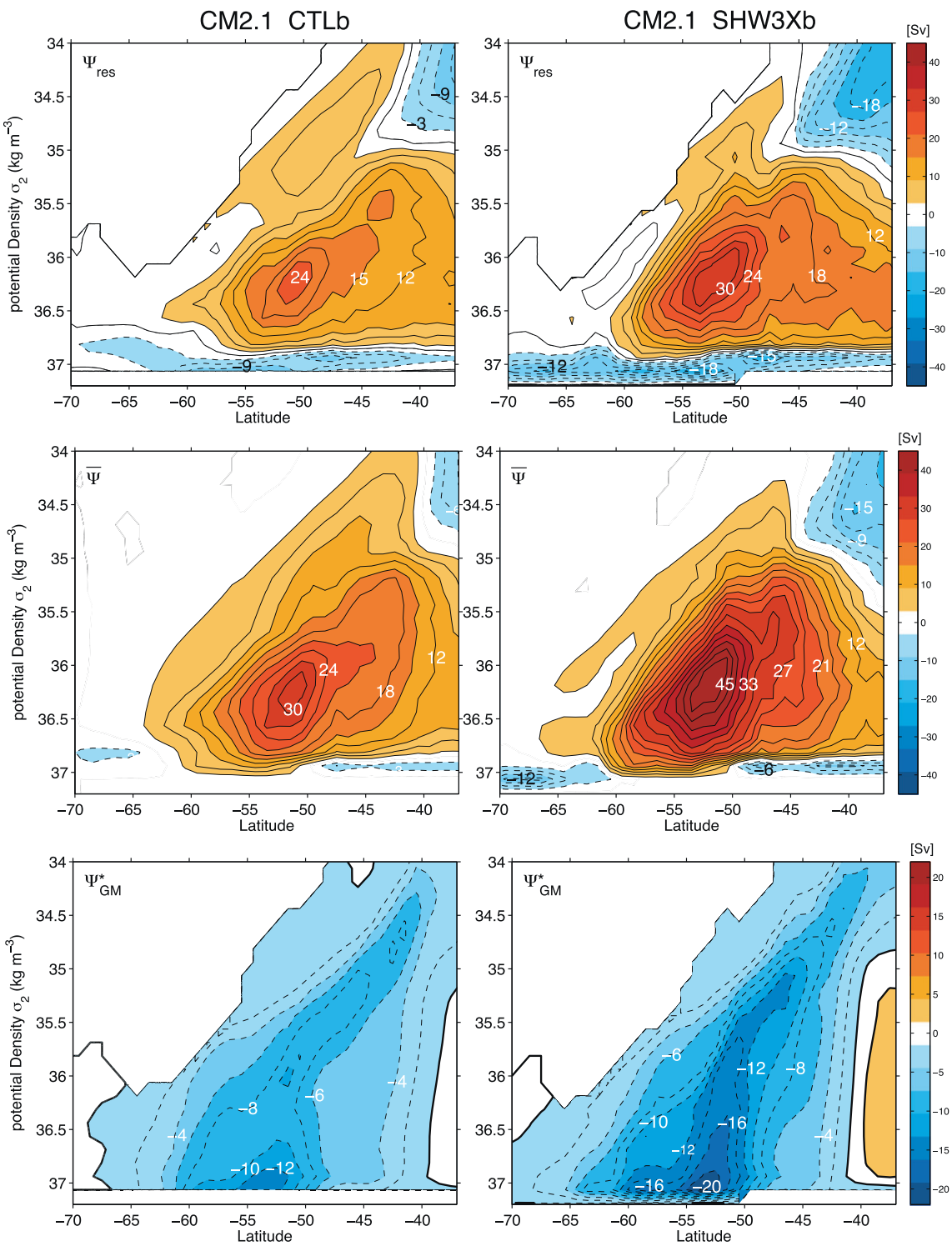


**Fig. 7.** MOC (Sv) in $\sigma_2$ density space for (left) CTLb and (right) SHW3Xb experiments: (top) the residual meridional circulations $\Psi_{res}$, (middle) the contributions from the Eulerian transport $\overline{\Psi}$, and (bottom) the contributions from the bolus transports $\Psi^*$. Transports are time-mean averages between model years 36–40 after the perturbed winds are imposed.

resulting in $\Psi_{res}$ strengthening by 14 Sv. Table 4 summarises the changes to the overturning circulation based on the two CM2.1 control parameters and CM2.4. Although SHW3Xb simulates a much stronger eddy response to strengthening wind stresses, CM2.1 behaviour is still significantly different from the eddy-permitting CM2.4, which shows a stronger $\Psi^*$ increase leading to a $\Psi_{res}$ change of only 3 Sv. This is a circulation sensitivity of roughly 45% and 20% of that found with CM2.1 CTLb and CTLa, respectively. The anomalous Ekman transport that is not balanced locally by eddy-induced circulation is responsible for a volume flux in the upper ocean that penetrates into the other ocean basins. The resulting circulation anomaly is shown in Fig. 8, where the difference in global MOC (SHW3Xb-CTLb) averaged for the interval 36–40 years after the perturbed winds are imposed is computed.

**Table 4**
Changes in the different contributions to the MOC (in Sv) for the perturbation experiments based on different GM parameters. SHW3Xa is based on CTLa (with $\kappa = 600\ m^2\ s^{-1}$ and $S_{max} = 1/500$) and SHW3Xb on CTLb (with $\kappa = 1200\ m^2\ s^{-1}$ and $S_{max} = 1/100$). The column CM2.4 refers to the same perturbation experiment performed with the eddy-permitting model.

| MOC | SHW3Xa | SHW3Xb | CM2.4 |
|---|---|---|---|
| $\Psi_{res}$ | 14 | 7 | 3 |
| $\overline{\Psi}$ | 15 | 15 | 14 |
| $\Psi^*$ | 1 | 8 | 11 |

Fig. 8 represents a strengthening of the global MOC with an enhanced flow of North Atlantic Deep Water (NADW) into the Southern Ocean. Farneti and Delworth (2010) showed that—for the same time period and roughly consistent with estimates of changes to the Southern Ocean $\Psi_{res}$—the enhanced transport at 30° S is approximately 13 Sv and 3 Sv for CM2.1 and CM2.4, respectively. CM2.1 CTLb shows a similar behaviour with an anomalous transport of around 6 Sv (Fig. 8), again consistent with changes to $\Psi_{res}$ in the Southern Ocean.

We now examine the behaviour of the ACC horizontal transport in the model. Subject to SHW3X forcings, CM2.4 was shown to be in an eddy-saturated regime (Straub, 1993), where eddies transform the additional energy input by the winds into eddy kinetic energy through baroclinic instability processes, resulting in a horizontal flow relatively insensitive to wind stress changes (Fig. 5d in Farneti et al. (2010)). The ACC transport in the model is computed as the volume transport (in Sv) through the Drake Passage and is plotted in Fig. 9 for the two controls and respective wind-perturbation experiments. As noted in Section 3.1 the climatological value of the ACC transport in CTLb is reduced by ~10 Sv due to the larger $\kappa$, and the sensitivity to SHW3X winds does not differ much between the two simulations. After 100 years of simulation the transport of SHW3Xa and SHW3Xb is only 10 Sv apart, approximately the climatological difference. The sensitivity of the ACC to doubling wind stress is on the order of 50 Sv for both CM2.1 experiments, while CM2.4 showed an acceleration in the mean flow of less than 10 Sv. However, although the response looks very similar in the two 100 year long experiments, the equilibrium values might be significantly different, with SHW3Xb resulting in a somewhat weaker acceleration of the zonal flow. In the zonally unbounded Southern Ocean, a diapycnal transfer of momentum by eddies is

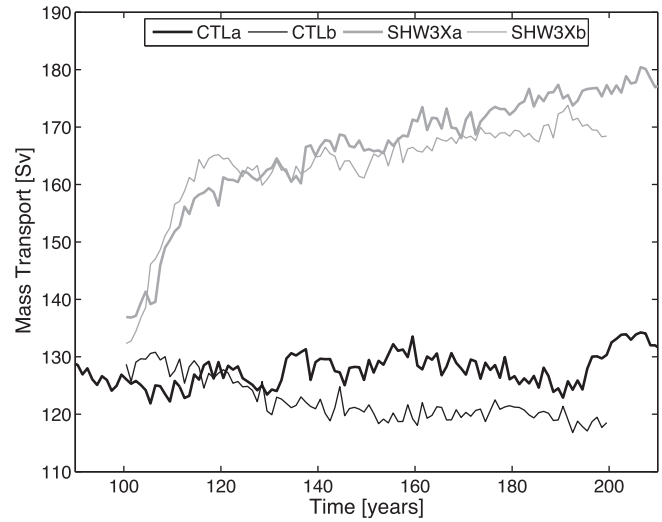


**Fig. 9.** Annual mean Drake Passage volume transport (Sv) for the GFDL CM2.1 coupled model. Experiments shown are the two control runs (CTLa, black solid line and CTLb, black thin line) and the perturbation runs with increased Southern Hemisphere winds (SHW3Xa, grey solid line and SHW3Xb, grey thin line). Note the initial jump in transport under SHW3X forcing.

the only mechanism able to balance the wind-stress input at the surface. Through interfacial form stress, eddies transfer momentum downwards that is eventually removed by bottom form stress over topographical obstacles (Hallberg and Gnanadesikan, 2001; Olbers et al., 2004). The response of the ACC's zonal transport to changes in wind stress forcing appears to depend strongly on the representation of both standing and transient eddies in fluxing momentum vertically. This mechanism, when compared with CM2.4, is clearly not well reproduced by the eddy-flux closure in CM2.1 simulations. It is also possible that the reasons for this might transcend the role of GM, as a too-viscous flow could cause too-weak eddies, preventing a fast connection between momentum input at the surface and pressure torque at the bottom.

Finally, we consider an aspect of the consequences for the climate system originating from the different physical simulations in the two models. Wind-driven deep upwelling and associated ventilation of the sub-surface waters rich in carbon have a key role in the variability of $CO_2$ flux. The Southern Ocean provides a major

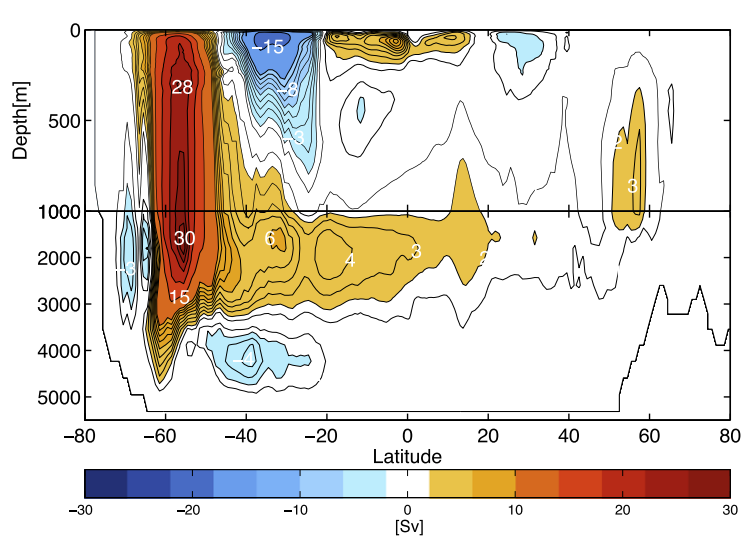


**Fig. 8.** Difference in MOC between the perturbation experiment SHW3Xb and the control run CTLb. For comparison with CM2.4 results, differences are computed for years 36–40 after the perturbed winds are imposed.

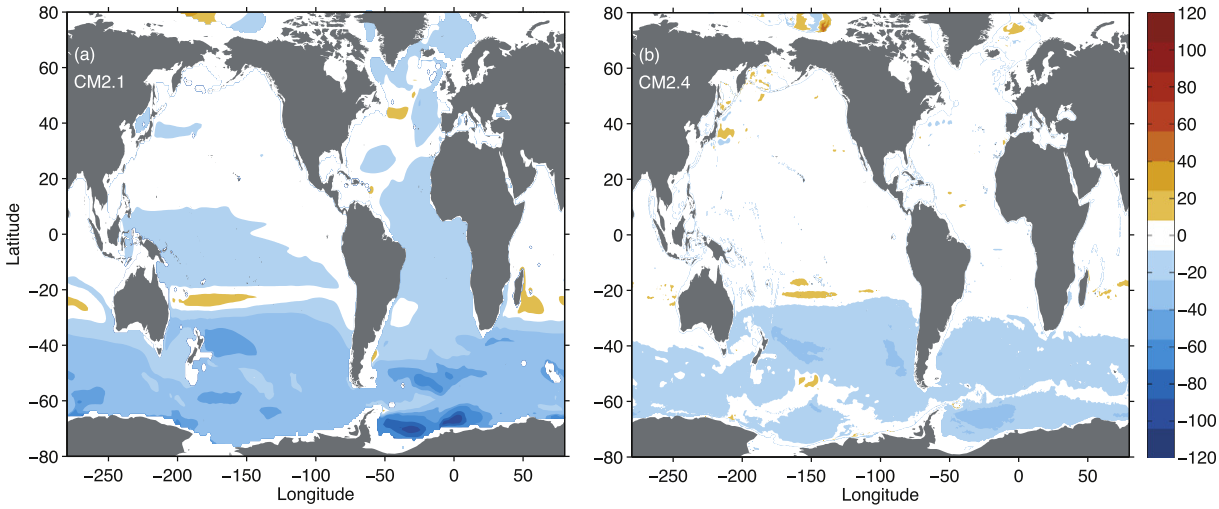


**Fig. 10.** Change in ideal age at 800 m depth for (a) CM2.1 CTLb and (b) CM2.4 due to SHW3X wind stress forcing. Differences are computed for years 36–40 after the perturbed winds are imposed. Blue colours mean younger waters (higher ventilation/upwelling) and red colours older waters (weaker ventilation/upwelling).

sink for anthropogenic $CO_2$ (Gruber et al., 2009) and changes in its circulation resulting from enhanced westerly winds have been identified as a dominant cause of atmospheric $CO_2$ change (Le Quéré et al., 2007). A tracer of ventilation age present in numerical models, ideal age, is used to study changes in ventilation during the SHW3X integrations in the models (see also Bryan et al. (2006)). Under global warming conditions, an increase in ideal age is expected due to higher stratification and induced weakening ventilation (Gnanadesikan et al., 2007b). However, the sole effect of intensified SH winds would be to increase ocean ventilation through an enhanced upwelling of NADW in the Southern Ocean. We show in Fig. 10 the change in ideal age at a depth of 800 m in the modified CM2.1 and CM2.4 models. The modified CM2.1 used in this work exhibits an increase in deep-upwelling, and thus ventilation leading to younger waters, throughout the Southern Ocean region. Further, it is notable that significant anomalies are present in the North Atlantic basin. CM2.4, in contrast, displays a considerable weaker sensitivity, with only minor and local alterations of ventilation rates. Thus, a correct representation of enhanced eddy fluxes in future climates is crucial for the projection of future trends in air-sea fluxes of carbon.

## 4. Discussion and conclusions

Present day control runs and runs with a large increase in the zonal wind stress in the SH over the ACC have been run in three different versions of GFDL climate models. In the CM2.4 SHW3X run, where the maximum zonal wind stress is doubled compared to the control run, the maximum of the MOC near the ACC and the density structure across the ACC do not change much on interdecadal time scales. This means that the eddy-induced MOC ($\Psi^*$) increases significantly to oppose the increase in the mean flow MOC ($\overline{\Psi}$) due to the much stronger northward Ekman flow. The CM2.4 ocean component has eddy permitting resolution, which is about 15 km near the ACC, rather than eddy resolving resolution of 0.1° or finer. Despite this defect, we assume that climate models that use non-eddy-resolving ocean resolution, where the eddy effects are parameterized, should show a response to SHW3X forcing similar to that of CM2.4.

If the eddies are parameterized using GM, then the strength of $\Psi^*$ depends upon the coefficient $\kappa$ and the local density gradients in the ocean component. Given that the density structure in the CM2.4 control and SHW3X runs is very similar across the ACC, then $\Psi^*$ can only increase significantly by a large increase in $\kappa$. Therefore, our first conclusion is that climate models that use a constant $\kappa$ will get the wrong response for the future climate if the zonal wind stress over the ACC changes. The magnitude of the incorrect response will depend on the size of the change in the zonal wind stress. For example, the CCSM3, which uses a constant $\kappa$, will only have a small error because Goes et al. (2008) show that the zonal wind stress only increases by 3% over the 21st Century under the A1B scenario forcing. In contrast, Delworth and Zeng (2008) show that the CM2.1 model has quite a large increase in zonal wind stress over the 21st Century using the same scenario. A majority of the ocean components in IPCC AR4 climate models used a constant $\kappa$ in the GM parameterization, including the CCSM3, and these components should be improved by using a $\kappa$ that is allowed to vary.

It is clear from Farneti et al. (2010) that the response of the original CM2.1 model to SHW3X forcing differs markedly from the CM2.4 response. $\Psi^*$ is nearly the same as in the control run, so that the residual transport $\Psi_{res}$ increases significantly because the northward Ekman flow is almost doubled. This leads to much larger slopes of the isopycnals across the ACC, and consequently to a much higher transport through Drake Passage. The reason is the small value of $S_{max}$ set to 1/500 and an upper limit of 600 $m^2\,s^{-1}$ on $\kappa$. Griffies et al. (2005) discusses the reason for these choices: "The diffusivity times the maximum slope represents a maximum volume flux associated with GM. This product determines an upper limit on what parameterized eddies can do in countering wind-driving Ekman fluxes. Given that Ekman volume fluxes are of order 1 $m^2\,s^{-1}$, we chose not to let the parameterized fluxes greatly exceed this value." Thus, the values were set based on the present day control run conditions, and are clearly not large enough for the SHW3X run near the ACC where the maximum zonal wind stress and resulting Ekman flow are doubled. Therefore, our second conclusion is that putting limits on physical parameterization coefficients can compromise results when the parameterizations are pushed up against those limits. The CM2.1 is a good example of this because the GM $\kappa$ had a variable definition, but the results of the A1B scenario 21st Century run, which had a significant increase in the zonal winds over the ACC, are compromised by the upper limit of 600 $m^2\,s^{-1}$ on $\kappa$. Farneti and Delworth (2010) show that the ocean results are not just compromised near the ACC, but CM2.1 shows differences from CM2.4 in the global ocean

circulation, and especially in the important heat transport due to the MOC in the North Atlantic Ocean. Note that all climate models using a constant $\kappa$, such as the CCSM3, are also compromised in this way.

In this paper, control and SHW3X run results have been presented with a modified version of CM2.1, where the $S_{max}$ has been increased to 1/100 and the maximum $\kappa$ value increased to $1200\,m^2\,s^{-1}$. This has allowed their product, which is the upper limit of what parameterized eddies can do, to be an order of magnitude higher than in the original version. Table 3 shows that the CTLb run using these larger values is considerably worse in some important measures when compared to the CTLa run, which is why the original smaller numbers were chosen. For the modified CM2.1, a larger cap than $1200\,m^2\,s^{-1}$ could have been chosen, but that would have resulted in even larger changes in a control run. The modified CM2.1 does a better job in responding to the SHW3X forcing, but still does not respond in quite the same way as CM2.4. The eddy-induced MOC near the ACC increases quite substantially over that in the control run, but not enough to completely balance the increase in the mean flow MOC due to the nearly doubled Ekman flow. This results in a small change to the density structure that produces an increase in the transport through Drake Passage. Therefore, our third conclusion is that the GM implementation where $\kappa$ is set proportional to the vertically averaged horizontal density gradient and has no vertical variation, does not produce quite a large enough $\kappa$ when the maximum zonal wind stress over the ACC is doubled from the present day value. This conclusion using a state-of-the-art climate model is similar to the conclusion in Viebahn and Eden (2010), who used an idealized model with a constant depth, no topography and very simple geometry. They used a different implementation of GM following the simplified, diagnostic treatment proposed in Eden and Greatbatch (2008), where $\kappa$ is specified locally using the Eady growth rate and a length scale which is the minimum of the Rossby radius of deformation and the Rhines scale.

The obvious question is what can be done to the specification of the GM $\kappa$ so that the parameterized eddies respond better to a large increase in zonal wind stress? There are two lines of progress that are likely ways forward. The first is that two different methods to taper $\kappa$ near the ocean surface have now been implemented in ocean climate components that are much better physically based than the slope clipping method using $S_{max}$ in the CM2.1. The first has been implemented in the ocean component of the CCSM4, with improved solutions documented in Danabasoglu et al. (2008). It involves a transition layer between the mixed layer, where the eddy-induced velocity has no vertical shear and there is horizontal diffusion, and the deeper ocean where GM is applied. The second is based on an assumed vertical mode structure and has been implemented in the GFDL ocean component, see Ferrari et al. (2010). The second line of progress is to implement a formulation for $\kappa$ so that it more directly responds to the strength of the wind stress. One possibility is to carry the eddy kinetic energy as a new model variable, which has been proposed by both Eden and Greatbatch (2008) and Marshall and Adcroft (2010). The production term in the equation for eddy kinetic energy depends directly on the wind stress, and so could produce large eddy energy in the ACC region, although $\kappa$ would only vary as the square root of the eddy kinetic energy. It remains to be seen whether this way of defining $\kappa$ would produce a more sensitive eddy-induced MOC when a large increase in zonal wind stress is applied over the ACC region.

## Acknowledgements

This study is based on model integrations that were performed at the NOAA/GFDL supercomputing facilities when the first author was a postdoc there. The support of the Climate Group at GFDL is gratefully acknowledged. NCAR is sponsored by the National Science Foundation. Stephen M. Griffies and two anonymous reviewers made useful and constructive comments on the manuscript.

## References

Bryan, F.O., Danabasoglu, G., Gent, P.R., Lindsay, K., 2006. Changes in ocean ventilation during the 21st Century in the CCSM3. Ocean Modell. 15, 141–156.
Danabasoglu, G., Ferrari, R., McWilliams, J.C., 2008. Sensitivity of an ocean general circulation model to a parameterization of near-surface eddy fluxes. J. Climate 21, 1192–1208.
Danabasoglu, G., Marshall, J., 2007. Effects of vertical variations of thickness diffusivity in an ocean general circulation model. Ocean Modell. 18, 122–141.
Delworth, T.L., Zeng, F., 2008. Simulated impact of altered Southern Hemisphere winds on the Atlantic meridional overturning circulation. Geophys. Res. Lett. 35, L20708. doi:10.1029/2008GL035166.
Eden, C., 2006. Thickness diffusivity in the southern ocean. Geophys. Res. Lett. 33 (11). doi:10.1029/2006GL026157.
Eden, C., Greatbatch, R., 2008. Towards a mesoscale eddy closure. Ocean Modell. 20, 223–239.
Eden, C., Jochum, M., Danabasoglu, G., 2009. Effects of different closures for thickness diffusivity. Ocean Modell. 26, 47–59.
Farneti, R., Delworth, T.L., 2010. The role of mesoscale eddies in the remote oceanic response to altered Southern Hemisphere winds. J. Phys. Oceanogr. 40 (10), 2348–2354.
Farneti, R., Delworth, T.L., Rosati, A.J., Griffies, S.M., Zeng, F., 2010. The role of mesoscale eddies in the rectification of the Southern Ocean response to climate change. J. Phys. Oceanogr. 40 (7), 1539–1557.
Ferrari, R., Griffies, S.M., Nurser, A.J.G., Vallis, G.K., 2010. A boundary-value problem for the parameterized mesoscale eddy transport. Ocean Modell. 32 (3–4), 143–156.
Ferreira, D., Marshall, J., Hemibach, P., 2005. Estimating eddy stresses by fitting dynamics to observations using a residual-mean ocean circulation model and its adjoint. J. Phys. Oceanogr. 35, 1891–1910.
Ganachaud, A., Wunsch, C., 2003. Large-scale ocean heat and freshwater transports during the World Ocean Circulation Experiment. J. Climate 16, 696–705.
Gent, P.R., McWilliams, J.C., 1990. Isopycnal mixing in ocean circulation models. J. Phys. Oceanogr. 20, 150–155.
Gent, P.R., Willebrand, J., McDougall, T.J., McWilliams, J.C., 1995. Parameterizing eddy-induced tracer transports in ocean circulation models. J. Phys. Oceanogr. 25, 463–474.
Gillette, N.P., Thompson, D.W.J., 2003. Simulation of recent Southern Hemisphere climate change. Science 302, 273–275.
Gnanadesikan, A., 1999. A simple predictive model for the structure of the oceanic pycnocline. Science 283, 2077–2079.
Gnanadesikan, A., Dixon, K.W., Griffies, S.M., Balaji, V., Barreiro, M., Beesley, J.A., Cooke, W.F., Delworth, T.L., Gerdes, R., Harrison, M.J., Held, I.M., Hurlin, W.J., Lee, H.C., Liang, Z., Nong, G., Pacanowski, R.C., Rosati, A., Russell, J., Samuels, B.L., Song, Q., Spelman, M.J., Stouffer, R.J., Sweeney, C.O., Vecchi, G., Winton, M., Wittenberg, A.T., Zeng, F., Zhang, R., Dunne, J.P., 2006. GFDL's CM2 global coupled climate models. Part II: the baseline ocean simulation. J. Climate 19 (5), 675–697.
Gnanadesikan, A., Griffies, S.M., Samuels, B.L., 2007a. Effects in a climate model of slope tapering in neutral physics schemes. Ocean Modell. 16, 1–16.
Gnanadesikan, A., Russell, J.L., Zeng, F., 2007b. How does ocean ventilation change under global warming? Ocean Sci. 3, 43–53.
Goes, M., Wainer, I., Gent, P.R., Bryan, F.O., 2008. Changes in subduction in the South Atlantic ocean during the 21st century in the CCSM3. Geophys. Res. Lett. 35, L06701. doi:10.1029/2007GL032762.
Griffies, S., 1998. The Gent-McWilliams skew-flux. J. Phys. Oceanogr. 28, 831–841.
Griffies, S.M., Gnanadesikan, A., Dixon, K.W., Dunne, J.P., Gerdes, R., Harrison, M.J., Rosati, A., Russell, J.L., Samuels, B.L., Spelman, M.J., Winton, M., Zhang, R., 2005. Formulation of an ocean model for global climate simulations. Ocean Sci. 1, 45–79.
Gruber, N., Gloor, M., Mikaloff, F.S.E., Doney, S.C., Dutkiewicz, S., Follows, M.J., Gerber, M., Jacobson, A.R., Joos, F., Lindsay, K., Menemenlis, D., Mouchet, A., Müller, S.A., Sarmiento, J.L., Takahashi, T., 2009. Oceanic sources, sinks, and transport of atmospheric $CO_2$. Global Biogeochem. Cycles 23 (1). doi:10.1029/2008GB003349.
Hallberg, R., Gnanadesikan, A., 2001. An exploration of the role of transient eddies in determining the transport of a zonally reentrant current. J. Phys. Oceanogr. 31, 3312–3330.
Ivchenko, V.O., Danilov, S., Olbers, D., 2008. Eddies in numerical models of the Southern Ocean. In: Hecht, M.W., Hasumi, H. (Eds.), In: Ocean modelling in an eddying regime, AGU Geophysical Monograph Series, vol. 177. pp. 177–198.
Karsten, R., Marshall, J., 2002. Constructing the residual circulation of the ACC from observations. J. Phys. Oceanogr. 32, 3315–3327.
Kushner, P.J., Held, I.M., Delworth, T.L., 2001. Southern Hemisphere atmospheric circulation response to global warming. J. Climate 14, 2238–2249.
Le Quéré, C., Rödenbeck, C., Buitenhuis, E.T., Conway, T.J., Langenfelds, R., Gomez, A., Labuschagne, C., Ramonet, M., Nakazawa, T., Metzl, N., Gillett, N., Heimann, M., 2007. Saturation of the Southern Ocean $CO_2$ sink due to recent climate change. Science 316, 1735–1738.

Marshall, D.P., Adcroft, A., 2010. Parameterization of ocean eddies: vorticity mixing, energetics and Arnold's first stability theorem. Ocean Modell. 32, 188–204.

Marshall, J., Radko, T., 2003. Residual-mean solutions for the Antarctic Circumpolar Current and its associated overturnig circulation. J. Phys. Oceanogr. 33, 2341–2354.

Mignone, B.K., Gnanadesikan, A., Sarmiento, J.L., Slater, R.D., 2006. Central role of Southern Hemisphere winds and eddies in modulating the oceanic uptake of anthropogenic carbon. Geophys. Res. Lett. 33, L01604. doi:10.1029/2005GL024464.

Olbers, D., Borowski, D., Völker, C., Wölff, J.-O., 2004. The dynamical balance, transport and circulation of the Antarctic Circumpolar Current. Ant. Sci. 16 (4), 439–470.

Reynolds, R.W., Rayner, N., Smith, T.M., Stokes, D., Wang, W., 2002. An improved *in situ* and satellite SST analysis for climate. J. Climate 15, 1609–1625.

Rintoul, S., Hughes, C., Olbers, D., 2001. The Antarctic Circumpolar Current system. In: Siedler, G., Church, J., Gould, J. (Eds.). Academic Press, pp. 271–302. Chapter 4.6.

Russell, J.L., Dixon, K.W., Gnanadesikan, A., Stouffer, R.J., Toggweiler, J.R., 2006. The Southern Hemisphere westerlies in a warming world: propping open the door to the deep ocean. J. Climate 19 (24), 6382–6390.

Sloyan, B.M., Kamenkovich, I.V., 2007. Simulation of subantarctic mode and Antarctic intermediate waters in climate models. J. Climate 20, 5061–5080.

Steele, M., Morfley, R., Ermold, W., 2001. PHC: a global ocean hydrography with a high-quality Arctic ocean. J. Climate 14, 2079–2087.

Straub, D.N., 1993. On the transport and angular momentum balance of channel models of the Antarctic Circumpolar Current. J. Phys. Oceanogr. 23, 776–782.

Treguier, A.M., Held, I.M., Larichev, V.D., 1997. Parameterization of quasigeostrophic eddies in primitive equation ocean models. J. Phys. Oceanogr. 27 (4), 567–580.

Trenberth, K., Caron, J.M., 2001. Estimates of meridional atmosphere and ocean heat transports. J. Climate 14, 3433–3443.

Viebahn, J., Eden, C., 2010. Towards the impact of eddies on the response of the Southern ocean to climate change. Ocean Modell. 34, 150–165.

Visbeck, M., Marshall, J., Haine, T., Spall, M., 1997. Specification of eddy transfer coefficients in coarse-resolution ocean circulation models. J. Phys. Oceanogr. 27, 381–402.